SAND2011-7123C

# CYLINDRICAL RAMP COMPRESSION EXPERIMENT ANALYZED WITH SURFACE FITTING METHODOLOGY

**M.R. Martin*, R.L. Lemke*, R.D. Mcbride*, J-P Davis* and M.D. Knudson***

**Sandia National Laboratories, Albuquerque, NM 87111*

**Abstract.** The shockless compression of a cylindrical liner Z-pinch is explored as a method to obtain high pressure (10's of Mbar) states while minimizing the entropy production in the target material. Experiments with beryllium liners on the Z-machine resulted in radiographic profiles at four different times in the liner's trajectory. From these results, we infer the longitudinally and azimuthally averaged material density, material pressure, and magnetic pressure along with their uncertainties. By combining these results with magnetohydrodynamic simulation, we obtain a pressure versus density response in solid beryllium up to 2.4 Mbar. We conclude that the pressure versus density response for material samples in the 10 Mbar range is achievable on the Z-machine with improved radiographic capability.

**Keywords:** shockless compression, z-pinch, cylindrical convergence, beryllium

## INTRODUCTION

Pulsed power drivers, such as the Z-machine at Sandia National Labs[1], have recently been utilized as platforms for performing dynamic materials experiments[2, 3]. The ability to achieve megabar drive pressures with a magnetic field, along with the capability to control the shape of the current drive over many hundreds of nanoseconds, has proved valuable for both shock[4, 5] and ramp compression[6] experiments in the high energy density regime. The bulk of these magnetically driven dynamic materials experiments on Z have been performed in divergent geometries[7, 8] for which $P \propto \frac{I^2}{L_0}$ where $P$ is the drive pressure, $I$ is the drive current, and $L_0$ is a constant scale factor dependent upon the initial geometry of the system. In this configuration, the current carrying anode and cathode are pushed away from each other and the drive pressure will never exceed this idealized scaling. However, for dynamic materials experiments performed in a convergent magnetic geometry, $P \propto \frac{I^2}{r}$, where $r$ is the radius of the current sheet. In cylindrical geometry, this is commonly referred to as a Z-pinch and its application to ramp and shock compression experiments on sub-microsecond time scales remains unexplored. In this paper, we present and analyze experimental results for convergent ramp compression experiments on the Z-machine in a cylindrical Z-pinch configuration. The geometric convergence inherent in this load design has the potential to increase the maximum achievable drive pressure, as compared to divergent geometries, in magnetically driven ramp compression experiments. However, the convergent nature of the target also makes diagnostic access of the sample more difficult and precludes the use VISAR diagnosed multi-sample techniques currently utilized on the Z-machine. These difficulties associated with convergent geometries necessitate the development of new diagnostic and analysis techniques to determine the pressure in the sample. We now briefly discussion the experimental results and present an analysis technique that allows for the inference of the sample pressure from multi-frame monochromatic backlighting of an imploding cylinder.

## EXPERIMENT AND ANALYSIS

The target is an aspect ratio four beryllium liner with an initial inner radius of $0.239cm$, thickness of $800\mu m$, and is $0.65cm$ tall. The beryllium liner is directly driven with a current pulse shape with a time rate of change in the drive pressure avoids shock formation in the liner[4] and reaches a peak current of approximately $20MA$. This pulse shape is based on the LANL SESAME Be2020 equation of state. During the liner implosion, current flows on the outer surface of the liner and a magnetic diffusion front propagates radially inward toward the free surface, ahead of any thermal conduction. Eventually the magnetic diffusion front will contaminate the inner surface of the liner such as to limit the peak pressures achieved in the magnetic field free solid. A $1mm$ diameter tungsten rod is located inside the cylinder to serve as a fiducial and to limit self emission of the liner at stagnation. The imploding liner is diagnosed with a two-frame $6.1keV$ monochromatic radiography system[9] with $1ns$ temporal resolution. The detector is a Fuji BAS-TR2025 image plate which after six times magnification has a spatial resolution of order $15um$. Figure 1 shows the normalized transmission levels at the earliest and latest radiographed times. Since only two-radiographic frames are available per experiment, the experiment is performed twice with radiographic frames acquired at machine times $3.027\mu s$, $3.035\mu s$, $3.046\mu s$ and $3.050\mu s$. The load current of the two experiments was repeated to within 2 percent as determined by VISAR unfold[4].

Our goal is to infer the pressure-density state of the quasi-isentropically compressed liner inner surface from the experimental radiography. This approach is broken down in to two steps. The first step is to determine the mass densities and their uncertainties from the radiographs. Given the density profiles and their timings, we then directly integrate the mass and momentum conservation relations to determine the total pressure. This approach will ultimately lead to larger uncertainties in the inferred pressure state than is regularly achieved in a coaxial drive geometry. However, the convergent nature of the target makes fielding VISAR to measure the free surface velocity difficult and would limit the achievable pressures from convergence, so this precludes the use of characteristics based methods. Another complication arises since regions of the sample that have passed through the magnetic diffusion front have been Joule heated.

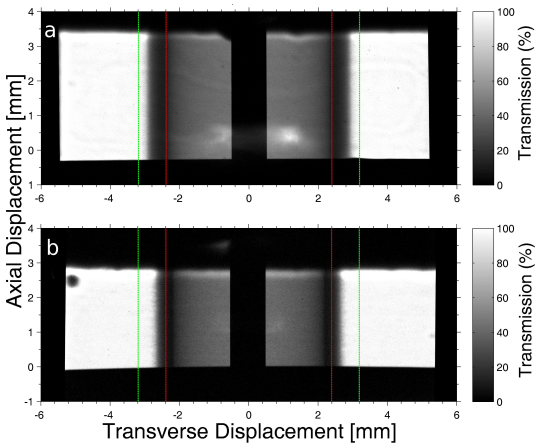


**FIGURE 1.** Radiograph transmission levels for the earliest and latest times of the ramp compressed beryllium cylinder at $a)3.027\mu s$ and $b)3.050\mu s$. The outer vertical and inner vertical lines denote initial outer and inner radii of the cylinder.

Since no diagnostic is available to determine the location of the magnetic diffusion front, we rely on Alegra[10] simulation to provide an upper bound on its radial location.

The first step in our analysis procedure is to determine the mass density versus radius from the image plate scans. The coordinate system and magnification factor for the experiment are determined from the know size and position of the tungsten rod on the axis. Next, the intensity gradients in the zero percent transmission fiducial region and one-hundred percent transmission region are removed by subtracting the least squares fit of a plane over each respective region. The image is then normalized to transmission, utilizing the tungsten rod region to define zero percent transmission and the region beyond the initial outer liner radius to define one-hundred percent transmission. Because each radial transmission line is has a low signal to noise ratio, the transmission levels are axially averaged over the height of the cylinder. This provides a mean intensity profile versus radius. We use the two-point Abel inversion of Dasch[11] to transform from the axially averaged radial intensity profile to an absorption coefficient $\mu$ with units of inverse length. The average opacity, $\overline{\kappa}$, of the liner is then determined from the mass of the

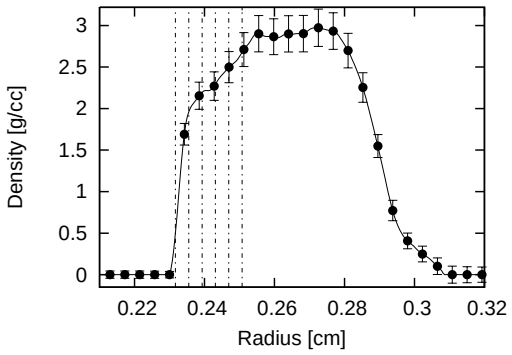


**FIGURE 2.** Abel inverted density profile from radiograph *a* in Figure 1. Dot-dash lines delineate the first five mass bins $m_i$ where $i \in \{0,4\}$ over the liner's inner surface.

cylinder's initial state $M_{liner}$ using equation 1.

$$\overline{\kappa} = \frac{M_{liner}}{\int^V \mu\,(r)\,dV} \tag{1}$$

The axially averaged mass density $\rho\,(r)$ is calculated by dividing the absorption coefficient $\mu$ by the average opacity $\overline{\kappa}$. In going from intensity to mass density, uncertainty analysis shows that the random error is dominated by the uncertainty in the average opacity value and the noise amplification from Abel inversion. The uncertainty in the mean opacity can be estimated from variation in equation 1 by propagating the uncertainties in the Abel inversion through the integral. The mean opacity increases in time and has a minimum value of $2.3\frac{cm^2}{g}$ in the first radiograph and a maximum value of $2.6\frac{cm^2}{g}$ in the final radiograph. The uncertainty in the Abel inversion is estimated through inverting each radial line in in the intensity profile before averaging and then calculating the standard error of the radial absorption profiles. The combined uncertainties for the density profile are shown in Figure 2 for the earliest radiograph. Each of the four frames gives an average uncertainty in the density of order eight percent and the inferred density profiles are consistent with Alegra simulation.

Given the radial density profiles and timings we now want to infer the total scalar pressure in the sample. The basis for this inference is to utilize a surface fitting methodology similar to reference[12]. This surface fitting procedure is performed under the assumption that the entropy increase due to plastic flow is negligible, that the experiment is independent of grain orientation, and that the implosion is axially symmetric. We begin by writing the equations for mass conservation (equation 2) and momentum conservation (equation 3) with respect to the material derivatives of the mass density $\rho$ and velocity $\mathbf{u}$, where $P$ is the scalar pressure. Our goal is the map the radial density profiles from the experiment onto a collocated mass grid and then numerically differentiate and integrate the equations in this transformed coordinate system.

$$\frac{D\rho}{Dt} = -\rho\nabla\cdot\mathbf{u} \tag{2}$$

$$\frac{D\mathbf{u}}{Dt} = -\frac{1}{\rho}\nabla P \tag{3}$$

Next we transform equations 2-3 into the mass coordinates using equation 4, where $L_z$ is the height of the cylinder.

$$dm = 2\pi L_z \rho r dr \tag{4}$$

This transformation to cylindrical mass coordinates gives the rate of change of the specific volume $v$ in terms of the radial velocity $u_r$ (equation 5) and the rate of change of radial velocity in terms of the total scalar pressure.

$$\frac{\partial v}{\partial t} = 2\pi L_z \frac{\partial\,(r u_r)}{\partial m} \tag{5}$$

$$\frac{\partial u_r}{\partial t} = -2\pi L_z r \frac{\partial P}{\partial m} \tag{6}$$

To numerically evaluate equations 5-6 the radial density profiles from the experiment are then mapped into a discrete mass coordinate system. Twenty bins of of equal mass $m_i$ are used to create the grid on which the specific volume will be time differentiated. The mapping to a mass coordinate is calculated with low-order numerical integration in conjunction with a root-finding scheme which repeatedly evaluates the integral from a starting coordinate $r_i$ to a $r_{i+1}$ such that $m_i = \frac{M_{total}}{nbin}$ The first five of these bins are marked by vertical lines in Figure 2. The uncertainty in the radial density profile limits the minimum $\delta M$ of the mapping since the uncertainty of the mapping is cumulative. This will ultimately limit the number of grid points available for calculating the

pressure. With each density profile mapped to a common coordinate system, we can now directly integrate the mass conservation and momentum conservation equations. The semi-discrete numerical form of these equations are given for radial velocity $u_r$ and total pressure $P$ in equations 7-8.

$$u_r(m_{i+1}) = \frac{1}{r}\int_{m_i}^{m_{i+1}} \frac{1}{2\pi L_z}\frac{\partial v}{\partial t} dm + u_r(m_i) \quad (7)$$

$$P(m_{i+1}) = -\int_{m_i}^{m_{i+1}} \frac{1}{2\pi L_z r}\frac{\partial u_r}{\partial t} dm + P(m_i) \quad (8)$$

The evaluation of the semi-discrete equations begins by approximating the radial velocity of the inner surface for bin $m_0$ with a cubic B-spline fit in time of the liner inner radius. This serves as the initial condition, $i = 0$, for integration of equation 7. Next, the time derivative of the specific volume is numerically evaluated for each mass bin $m_i$ by fitting a cubic B-spline through the four different times. Simpson's rule is then used to evaluate the integral over each bin from $m_i$ to $m_{i+1}$. After the radial velocity profile for each mass bin is determined, this procedure is repeated to determine the radial pressure profile. The inner surface pressure boundary condition for bin $m_0$ is assumed to be zero. Figure 3 shows a comparison between the Be2020 reference isentrope, the pressure unfold applied to the Alegra density profiles, and the unfolding procedure applied to the experimental density profiles. The unfold of from the simulation driven with the measured load current uses density profiles at the radiograph times of the experimet, the same timings of the radiographs, and the same total number of mass bins. The divergence of the inferred pressure from the isentrope for the simulated and experiment cases is consistent with the presence of magnetic field in the ablated portion of the liner. The magnetic pressure increases the total scalar pressure inferred since equation 8 makes no distinction between hydrodynamic and magnetic pressure. The uncertainties for the experimental pressure are estimated using Monte Carlo uncertainty analysis where the inputs to the pressure unfold procedure, the radial density profiles and radiograph times, are varied about their assumed normally distributed uncertainties. The variation in the inferred pressure is tracked and is shown in Figure 3 as a one sigma uncertainty.

We have presented the experimental results for ramp compression of a beryllium cylinder on the Z-Machine to approximately 2.4MBar. A procedure is presented for determining the mass densities along with their uncertainties from the experimental data. A surface fitting methodology is utilized in conjunction with Monte Carlo analysis to determine the samples pressure and corresponding uncertainties. Future, higher pressure, experiments are possible with a higher energy backlighter.

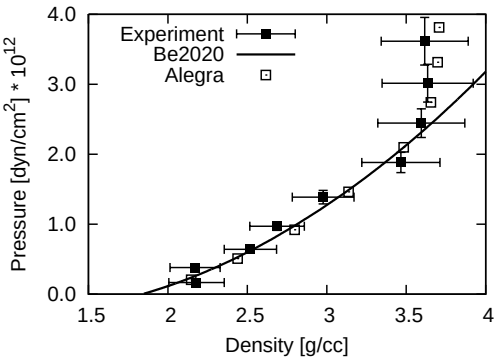


**FIGURE 3.** Plot of the reference Be2020 isentrope, surface fitting method applied to simulated density profiles, and surface fitting method applied to experimental density profiles. Divergence from the isentrope is due to magnetic pressure in the sample.

## ACKNOWLEDGMENTS

Sandia National Laboratories is a multi-program laboratory managed and operated by Sandia Corporation, a wholly owned subsidiary of Lockheed Martin Corporation, for the U.S. Department of Energy's National Nuclear Security Administration under contract DE-AC04-94AL85000.

## REFERENCES

1. Matzen, M. K., et al., *Phys. Plasmas*, **12**, 055503 (2005).
2. Reisman, D. B., et al., *J. Appl. Phys.*, **89**, 1625–1633 (2001).
3. Hall, C. A., et al., *Rev. Sci. Instrum.*, **72**, 3587–3595 (2001).
4. Lemke, R. W., et al., *J. Appl. Phys.*, **98**, 073530 (2005).
5. Knudson, M. D., et al., *Phys. Rev. Lett.*, **87**, 225501 (2001).

6. Hayes, D. B., et al., *J. Appl. Phys.*, **96**, 5520–5527 (2004).
7. Davis, J.-P., et al., *Phys. Plasmas.*, **12**, 056310 (2005).
8. Rothman, S. D., et al., *J. Phys. D*, **38**, 733 (2005).
9. Sinars, D. B., et al., *Rev. Sci. Instrum.*, **75**, 3672–3677 (2004).
10. Robinson, A. C., and Garasi, C. J., *Computer Physics Communications*, **164**, 408 – 413 (2004).
11. Dasch, C. J., *Appl. Opt.*, **31**, 1146–1152 (1992).
12. Aidun, J. B., and Gupta, Y. M., *J. Appl. Phys.*, **65**, 1898–1901 (1989).